Comprehending the Thermal Decomposition and Reconstruction Process of Sol–Gel MgAl Layered Double Hydroxides

ARTICLE *in* THE JOURNAL OF PHYSICAL CHEMISTRY C · JANUARY 2010

Impact Factor: 4.77 · DOI: 10.1021/jp910538r

7 AUTHORS, INCLUDING:

Jaime S Valente
Instituto Mexicano del Petroleo
96 PUBLICATIONS **1,591** CITATIONS
SEE PROFILE

Enrique Lima
Universidad Nacional Autónoma de México
103 PUBLICATIONS **1,046** CITATIONS
SEE PROFILE

Jose Toledo
Instituto Mexicano del Petroleo
5 PUBLICATIONS **55** CITATIONS
SEE PROFILE

Julia Prince
Anáhuac University
12 PUBLICATIONS **281** CITATIONS
SEE PROFILE

Comprehending the Thermal Decomposition and Reconstruction Process of Sol−Gel MgAl Layered Double Hydroxides

Jaime S. Valente,*,† Enrique Lima,‡ Jose A. Toledo-Antonio,† Maria A. Cortes-Jacome,† Luis Lartundo-Rojas,† Ramon Montiel,§ and Julia Prince||

Instituto Mexicano del Petróleo, 07730, Mexico, D.F., Mexico, Instituto de Investigaciones en Materiales, UNAM, 04510, Mexico D.F., Mexico, PEMEX-Petroquimica, I y D Tecnologico, 52500, Coatz. Ver., Mexico, and Universidad Autonoma Metropolitana-A, Quimica de Materiales, 02200, Mexico, D.F., Mexico

Received: November 4, 2009; Revised Manuscript Received: December 14, 2009

The evolution of MgAl layered double hydroxides (LDHs), prepared by the sol−gel method, throughout the synthesis−crystallization−calcination−reconstruction process is thoroughly studied and compared to a coprecipitated analogue. X-ray diffraction and transmission electron microscopy provide useful information about crystallinity and morphology of the samples. It was found that crystal sizes do not necessarily decrease after calcination−reconstruction. Furthermore, aluminum coordination is studied by ^{27}Al MAS nuclear magnetic resonance and by X-ray photoelectron spectroscopy (XPS), revealing significant differences in the relative populations of tetrahedral aluminum in the surface and the bulk of the calcined sol−gel LDHs. Magnesium and oxygen structural environments are also studied by XPS. A possible correlation between crystal sizes of calcined LDHs and the amount of O^{2-} surface species is discussed. Differences in the structural environment of magnesium in the as-synthesized and the reconstructed LDH are presented and analyzed.

1. Introduction

Layered double hydroxides (LDHs), also known as hydrotalcite-like compounds by reference to the naturally occurring hydrotalcite mineral, are a family of anionic clays that have received much attention in the past decades, for they have found numerous applications in many different fields.[1–3] For instance, LDHs have been used as antacids, PVC additives, flame retardants, and hybrid composites.[1] Also, considerable research has been conducted with the aim of intercalating drugs, biological species, and organic compounds, to use LDHs for controlled drug-delivery, as sensing devices, etc.[3] Furthermore, because of their basic properties, they have been extensively studied in heterogeneous catalysis, particularly in the synthesis of fine chemicals.[2,4]

The structure of an LDH is based on $M^{2+}(OH)_6$ octahedra that share edges to build $M(OH)_2$ brucite-like layers. An LDH is created by isomorphically substituting some M^{2+} for M^{3+} cations with similar ionic radius, rendering a positively charged layer. This charge is compensated by anionic species located in the interlayer region, along with hydration water molecules. LDHs are represented by the general formula: $[M_{(1-x)}{}^{2+}M_x{}^{3+}(OH)_2]^{x+}\ A_{x/n}{}^{n-}\cdot mH_2O$, where the divalent and trivalent cations may be Mg^{2+}, Zn^{2+}, Co^{2+}, Cu^{2+}, Ni^{2+}, Al^{3+}, Fe^{3+}, Ga^{3+}, Cr^{3+}, etc., A^{n-} may be nearly any organic or inorganic anion, and x is the trivalent cation substitution degree and takes values in the range $0.2 \leq x \leq 0.33$. Also, combinations of three or four cations have been reported. Therefore, a large number of materials with LDH structure and different physicochemical properties may be prepared.[1–3]

Usually, LDHs are synthesized by the coprecipitation of metallic salts with an alkaline solution.[1,2,5] However, alternative routes have been recently explored,[6–13] with the aim of a better control over the structural and textural properties, which are also related to the catalytic and anion exchange properties of LDHs. This has been achieved by means of various postsynthesis treatments, for instance, through microwave irradiation[6–8] or ultrasonic treatment.[6] Also, alternative synthesis procedures have been proposed, such as urea hydrolysis[7,8] and the sol−gel method.[9–12]

When an LDH is calcined, it progressively loses physisorbed water, then interlamellar water molecules, and finally water from the dehydroxylation of the layers, along with the charge-compensating anions, leading to the collapse of the layered structure. The temperatures at which these phenomena occur depend on the chemical composition; however, above 400 °C, a mixed oxide is formed.[1,2,14] In the case of Mg−Al LDHs, which are perhaps the most widely studied of this family, calcination produces an MgO phase, where the Al cations are presumed to be evenly distributed throughout the structure, creating a solid solution.[14] These Mg(Al)O mixed oxides have relatively high surface area (>200 $m^2\ g^{-1}$) and strong basic Lewis sites, O^{2-} atoms; hence, they have been successfully employed in many organic reactions catalyzed by bases.[15]

The oxides obtained by thermal decomposition of an LDH have the remarkable capacity of reconstituting the original layered structure upon adsorption of anions and water. This property is known as memory effect,[1,2] and it has been exploited for several applications of LDHs, such as adsorption of anionic contaminants from aqueous solutions[16] and SO_x removal.[17] Furthermore, if the calcined LDH is exposed only to water or water vapor for a certain time, the layered structure is reconstructed, admitting OH^- groups as charge-compensating anions. The Mg−Al−OH LDH is commonly known as meixnerite or meixnerite-like. The hydroxyls act as Brönsted basic sites in catalytic reactions.[18–21]

* To whom correspondence should be addressed. Phone: +52 (55) 9175-8444. E-mail: jsanchez@imp.mx.
† Instituto Mexicano del Petroleo.
‡ Instituto de Investigaciones en Materiales.
§ Pemex-Petroquimica.
|| Universidad Autonoma Metropolitana-A.

10.1021/jp910538r
Published on Web 01/12/2010

Given its numerous applications, much attention has been devoted to studying the calcination and reconstruction of LDHs.[22–34] However, further study is still required to understand the processes taking place. It has been observed that, during calcination, a significant amount of aluminum (~20%) changes to tetrahedral coordination. Therefore, there must be a small amount of an amorphous phase of spinel-based aluminas, such as γ-Al_2O_3, that cannot be detected by XRD.[22] As a result, the reconstruction of LDH from the MgO phase is not totally reversible. Hibino et al. found that the carbonate content (% weight), acting as charge-compensating anion, continuously decreases in subsequent calcination−rehydration cycles.[22] Furthermore, they found that spinel $MgAl_2O_4$ is formed from Mg−Al−CO_3 LDHs when calcination at 400 °C and subsequent reconstruction are repeated several times; spinel formation from a pure LDH requires calcination at temperatures above 800 °C.[22] These results indicate that some of the aluminum atoms are segregated and do not return to the LDH structure during reconstruction.

Magnesium, on the other hand, remains octahedrally coordinated through every step of the process; changes in the structural environment of magnesium are not easily detected and have been scarcely studied. Bokhoven et al. studied the coordination of the Mg centers by XAFS spectroscopy and determined that Mg has an identical, distorted octahedral coordination in the as-synthesized and the rehydrated LDH; they determined that, within the length-scale of XAFS, the reconstructed structure is identical to the as-synthesized materials.[23] However, there must be subtle changes in the structural environment of magnesium; some magnesium atoms must be interacting with the extracted aluminum, otherwise an alumina, not a $MgAl_2O_4$ spinel phase, would appear after several calcination and rehydration cycles.

Unobserved modifications to the environment of magnesium as well as that of aluminum after calcination−rehydration might also explain differences in the observed catalytic activity of meixnerite-like compounds, which have been hitherto attributed to changes in the rehydration procedure, the crystal size of the as-synthesized LDH, calcination time and temperature, etc. A number of studies have focused on studying the effect of crystal and particle size of the as-synthesized precursor on the catalytic activity of the meixnerite derivate.[24] Variations in crystal sizes are generally achieved by varying temperature and time of postsynthesis (e.g., hydrothermal) treatments. However, the extent to which crystallinity can be controlled by this method is limited; therefore, it is not yet clear to what extent crystallinity, morphology, and particle sizes are modified during calcination and rehydration.

The authors have previously reported the synthesis of pure MgAl LDHs by sol−gel method.[11] This method enables an accurate control over crystallinity and particle sizes, which can be fine-tuned over a very wide range.[12] Also, LDHs prepared following this methodology revealed peculiar nanocapsular morphology, in contrast to the classic platelet-like morphology of LDHs.[11,12] Therefore, these sol−gel LDHs provide a unique opportunity to study the calcination−reconstruction process. Changes in morphology, particle size, and crystallinity are analyzed, as well as the modifications of the structural environment of aluminum and magnesium, by X-ray diffraction, transmission electron microscopy, ^{27}Al MAS nuclear magnetic resonance, and X-ray photoelectron spectroscopy.

2. Experimental Methods

2.1. Synthesis Procedure. The synthesis procedure has been reported previously.[12] Briefly, LDHs were prepared by dissolving aluminum tri-*sec*-butoxide (ATB) in ethanol at 70 °C under constant stirring for 1 h. Nitric acid (3 M) was then added dropwise. After 1 h, the system was taken to room temperature, and acetic acid (AA) was added to complex the aluminum alkoxide. One hour later, the temperature was lowered to 0 °C, and magnesium methoxide was added dropwise. The system was stirred for 24 h at room temperature, and finally deionized water was added. The molar ratios of reactants were ATB:EtOH = 1:60, ATB:HNO_3 = 1:0.03, ATB:AA = 1:1, M^{2+}:M^{3+} = 3:1, and ATB:H_2O = 1:1. After the synthesis procedure was completed, the sols thus obtained were placed in a sealed digestion bomb and kept at 120 °C under autogenous solvent vapor pressure for 1−10 days. The samples were then dried at 100 °C.

MgAl-E corresponds to the sample with no postsynthesis treatment. The sample named MgAl-TH10 received a 10 day hydrothermal treatment. Another sample, labeled MgAl-TH1W, received a 24 h hydrothermal treatment; the sol was set in the presence of 50% vol. bidistilled water. As a comparison, sample MgAl-CP was prepared following the coprecipitation at low supersaturation method,[5] maintaining the pH constant at 9 and using nitrate salts as precursors.

Dried samples were calcined at two different temperatures for their analysis, 250 °C for 2 h and 550 °C for 4 h, with a heating rate of 2 °C/min. Reconstruction of the layered structure was performed by placing the calcined samples in a sealed container with 100% relative humidity for 10 days.

2.2. Characterization Techniques. ***X-ray Diffraction.*** The X-ray diffraction pattern of the samples was measured in a theta−theta Bruker D-8 Advance diffractometer with Cu Kα radiation, a graphite secondary-beam monochromator, and a scintillation detector. Diffraction intensity was measured between 4° and 80°, with a 2θ step of 0.02° and a counting time of 9 s per point.

Chemical Analysis. The chemical composition of solids was determined in a Perkin-Elmer model Optima 3200 Dual Vision by inductively coupled plasma atomic emission spectrometry (ICP-AES).

Electron Microscopy (TEM). Sample powders were characterized by high-resolution transmission electron microscopy (HRTEM) JEOL JEM-2200FS with Schotkky-type field emission electron gun operating at 200 kV. HRTEM digital images were obtained using a charged coupled device camera (CCD). The powdered samples were directly dry-sprayed onto commercially available amorphous holey film carbon-coated copper grid.

Solid-State Nuclear Magnetic Resonance. The single pulse solid-state ^{27}Al MAS NMR spectra were acquired under MAS conditions on a Bruker Avance 300 spectrometer, at a resonance frequency of 78.15 MHz. The samples were spun at 10 kHz. Short single pulses (π/12) with a repetition time of 0.5 s were used. Chemical shifts were referenced to an aqueous 1 N $AlCl_3$ solution.

Cross-polarization magic angle spinning solid-state ^{13}C NMR spectra were recorded at 75.422 MHz using a 4 mm cross-polarization (CP) MAS probe spinning at a rate of 5 kHz. Typical ^{13}C CP MAS NMR conditions for ^{1}H−^{13}C polarization experiment used a contact time of 4 ms and repetition time of 12 s for accumulation of 3000−5000 scans. Chemical shifts were referenced to the peak of solid adamantane at 38.2 ppm relative to TMS.

X-ray Photoelectron Spectroscopy. X-ray photoelectron spectra (XPS) were recorded on a THERMO-VG SCALAB 250 spectrometer equipped with Al Kα X-ray source (1486.6 eV)

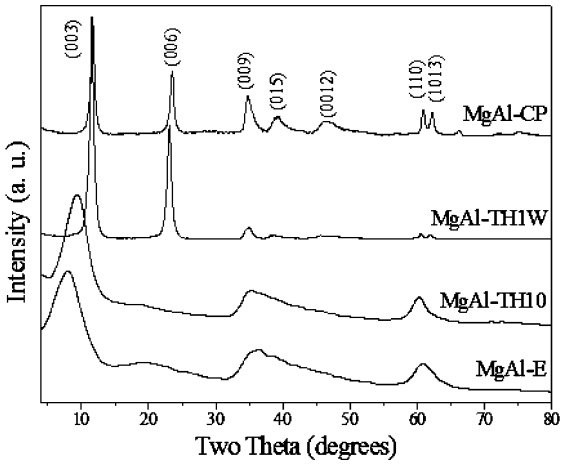

Figure 1. X-ray diffraction patterns of as-synthesized samples.

and a hemispherical analyzer. The base pressure during the analysis was 1.37×10^{-8} Pa. The XPS analyses were performed in a static system on the fresh, calcined, and rehydrated samples. The experimental peaks were decomposed into components using mixed Gaussian−Lorentzian functions, nonlinear squares fitting algorithm, and Shirley-type background subtraction by using XPS peak fit software. The C_{1s} line at 284.6 eV was used as an internal standard for the correction of binding energies (BE). Changes in the Al (2p) + Mg (2p) signal shape on the fresh, calcined, and rehydrated samples were analyzed by a curve-fitting procedure with peaks endowed using variable position, full width at half-maximum (fwhm), and intensities. Surface elemental composition was determined by fitting and integrating the Al_{2p}, Mg_{2p}, C_{1s}, and O_{1s} bands and converting these values to atomic ratios using theoretical sensitivity factors provided by the manufacturer of the XPS apparatus.[35] All XPS curves are shown with the differential fitting curve (lowest curve in each spectrum) after adjusting to theoretical curves. The calcination procedure was done in a Linkam cell, under flowing oxidizing atmosphere (air) in a dynamic thermal process, heating from 25 to 550 °C at a rate of 2 °C/min. Because of the memory effect, LDHs are easily reconstructed after calcination; thus, special care was taken. All manipulation of calcined samples was done under inert conditions using a glovebox and a special box vessel, attached to the XPS equipment, to introduce calcined samples into the ultra high vacuum chamber of the spectrometer.

3. Results

3.1. X-ray Diffraction. X-ray diffraction patterns of as-synthesized samples have been discussed previously.[12] For the sake of clarity, they are displayed in Figure 1. All samples have pure LDH structure. The characteristic peaks of the LDH phase, along with the corresponding Miller indices, are indicated for the MgAl-CP pattern. Significant differences are observed between this pattern and those of sol−gel samples. In MgAl-E, the 003 peak is shifted to a lower 2θ angle, indicating that the interlayer region is expanded by the intercalation of a large anion, which is most likely acetate (vide infra). Also, the wide peaks of the MgAl-E pattern indicate very small crystal sizes. For sample MgAl-TH10, the 003 peak's position is similar to that for MgAl-E; the peaks appear sharper as a consequence of crystal growth occurred during hydrothermal treatment. However, it is worth noting that crystal growth is indeed minor, for such a prolonged treatment. In contrast, MgAl-TH1W has an interlayer distance close to that of MgAl-CP, indicating that ethoxy groups have been displaced by carbonate anions trapped from the ambient. Furthermore, the peaks' sharpness is proof of a highly crystalline material. On the basis of these results, it is concluded that water is crucial for LDH crystal growth. Cell parameters *c* and *a*, which reflect the interlayer and cation−cation distances, were calculated from the 003 and 110 peak positions, assuming 3R stacking.[1] These are reported in Table 1, along with crystal sizes calculated using the Scherrer equation, by the fwhm of the 003 reflection.

It is a well-known fact that, by calcination of a MgAl LDH to temperatures above 400 °C, a mixed oxide is formed, commonly denoted as Mg(Al)O.[1] XRD of this mixed oxide presents the pattern of rock-salt like MgO, with the characteristic reflections slightly shifted because of the substitution of some Mg atoms with smaller Al atoms. In agreement with this, XRD of all calcined (at 550 °C) samples shows pure MgO phase, Figure 2. Crystal sizes were calculated by the fwhm of the 200 reflection. It is worth noting that, although crystal sizes still have the same tendency as in the as-synthesized samples, MgAl-TH1W > MgAl-CP > MgAl-TH10 > MgAl-E, the differences in crystallinity are less notorious.

After the calcined LDHs were kept in a moist environment, they recovered the original layered structure, as expected by the memory effect of these materials,[1] Figure 3. The reconstructed LDHs incorporate both OH^- groups and CO_3^{2-} from the ambient as charge-compensating anions. The interlayer distances (Table 1) are very similar among samples, indicating that they all have the same charge-balancing anions. Interlayer distances of carbonate and hydroxyl-intercalated LDHs are very similar,[1] so these anions are undistinguishable by XRD.

On the other hand, the *a* parameter, indicative of the cation−cation distance, is a function of the Mg/Al ratio and obeys Vegard's law.[1,36] As the Mg/Al ratio decreases, *a* decreases, because the radius of Al^{3+} is smaller than that of Mg^{2+}. As-synthesized samples had an Mg/Al molar ratio of ca. 2.5 (Table 1). The *a* value of all rehydrated samples agrees well with that reported for this composition,[36] within experimental error, indicating that there is no significant change in the Mg/Al molar ratio in the LDH phase during the calcination−rehydration process. The only exception is sample MgAl-TH10, whose bigger *a* value is indicative of magnesium enrichment in the LDH phase.

3.2. Transmission Electron Microscopy. Figure 4 shows transmission electron micrographs of three as-synthesized samples, MgAl-E, MgAl-TH1W, and MgAl-CP. MgAl-E presents the nanocapsular morphology that has been observed and discussed previously.[11] It has also been reported that after hydrothermal treatment with the mother liquor, that is, MgAl-TH10, the morphology does not change, but the nanocapsules grow and coalesce (not shown).[12] This morphology is restricted to nonaqueous systems; when the sol−gel LDH is submitted to a hydrothermal treatment under excess water (MgAl-TH1W), the morphology is drastically different, as it evolves into the platelet-like morphology that is characteristic of LDHs.[12] Furthermore, sample MgAl-CP prepared by conventional co-precipitation method has the same platelet morphology, as expected. High-resolution electron microscopy (insets in Figure 4a−b) revealed that both nanocapsular and the platelet morphologies exhibit a layered structure; interlayer distances are larger for MgAl-E than for MgAl-TH1W and for MgAl-CP, in agreement with the results obtained by XRD.

With treatment at 250 °C, the morphology of the samples presented modifications, as shown by the transmission electron micrographs of samples MgAl-E, MgAl-TH1W, and MgAl-CP presented in Figure 4d−f. In the case of the MgAl-E sample,

TABLE 1: Cell Parameters and Crystal Sizes for As-Synthesized, Calcined (550 °C), and Calcined−Rehydrated Samples

	unit cell parameters (Å)				crystal sizes (Å)[a]					
	as-synthesized		rehydrated		as-synthesized		calcined	rehydrated		
sample	*a*	*c*	*a*	*c*	L_{003}	L_{110}	L_{200}	L_{003}	L_{110}	Mg/Al molar ratio[b]
MgAl-E	3.089	28.110	3.048	23.129	18	56	34	48	90	2.53
MgAl-TH10	3.067	28.297	3.057	23.406	24	107	41	90	215	2.57
MgAl-TH1W	3.055	23.011	3.048	23.424	139	422	60	74	116	2.59
MgAl-CP	3.056	23.192	3.050	23.453	91	271	39	67	117	2.93

[a] Calculated applying the Scherrer equation to the indicated reflections. [b] Determined by inductively coupled plasma atomic emission spectrometry (ICP-AES) on the as-synthesized samples.

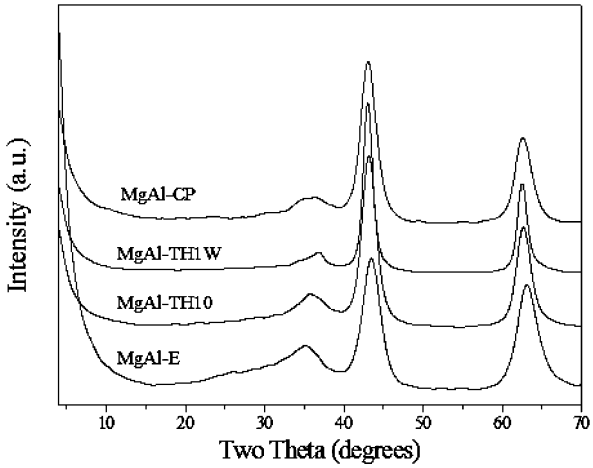

Figure 2. X-ray diffraction patterns of samples calcined at 550 °C.

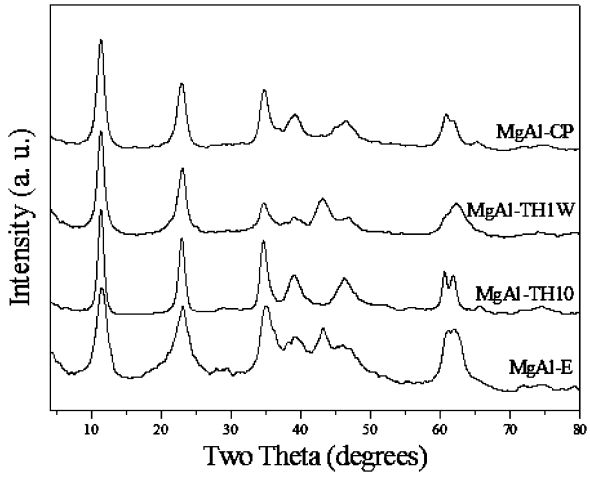

Figure 3. X-ray diffraction patterns of calcined (550 °C) and rehydrated samples.

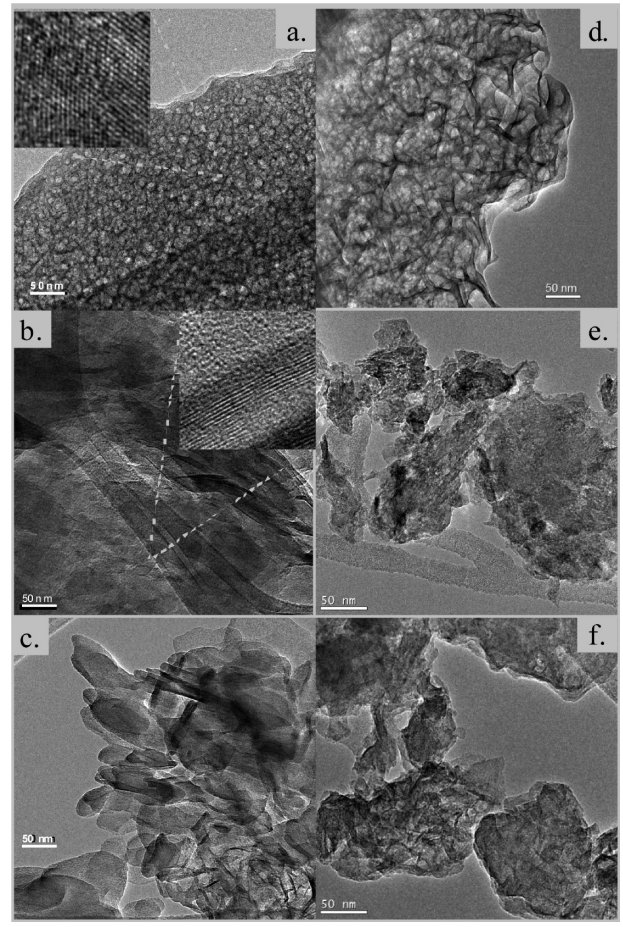

Figure 4. TEM micrographs of as-synthesized samples, (a) MgAl-E, (b) MgAl-TH1W, and (c) MgAl-CP, and samples thermally treated at 250 °C, (d) MgAl-E, (e) MgAl-TH1W, and (f) MgAl-CP.

the morphology is still nanocapsular, but the size of the capsules increased. For samples MgAl-TH1W and MgAl-CP, the platelet morphology has practically disappeared, and in certain regions we can observe the formation of microcrystalline domains.

After calcination at 550 °C, Figure 5, the formation of a polycrystalline material is clear in all samples. Calcined MgAl-E shows an agglomerate of small, globular particles. A similar morphology was observed on calcined MgAl-TH10 (not shown). Samples MgAl-TH1W and MgAl-CP, on the other hand, reveal a "house-of-cards" structure,[37] formed by collapse of the platelets, characteristic of calcined LDHs. In all cases, an MgO phase was observed by HRTEM, in agreement with XRD results and with previous reports (Figure 5b). However, in sample MgAl-E, a small number of nanocrystalline domains of γ-Al_2O_3 were also detected (Figure 5c).

When the calcined samples undergo a rehydration process, the morphology of the materials suffers a new modification, Figure 6. The nanocapsular morphology observed in the as-synthesized MgAl-E is not preserved; however, the morphology still bears differences from sample MgAl-CP. Even though both samples show an irregular stacking of platelets, MgAl-E presents some semispherical voids that remind us of its original morphology. Comparisons between direct measurements taken from the high-resolution micrographs, displayed as insets in Figure 6, and the interlayer spacing values reported in the X-ray powder data file (XRPDF 89-0460) reveal that both materials, rehydrated MgAl-E and MgAl-CP, present a not well-oriented layered structure.

3.3. Nuclear Magnetic Resonance. Figure 7 compares the ^{27}Al MAS NMR spectra of as-synthesized samples. Spectra were composed by an intense NMR signal close to 0 ppm, indicating the octahedral coordination of aluminum in the brucite-like

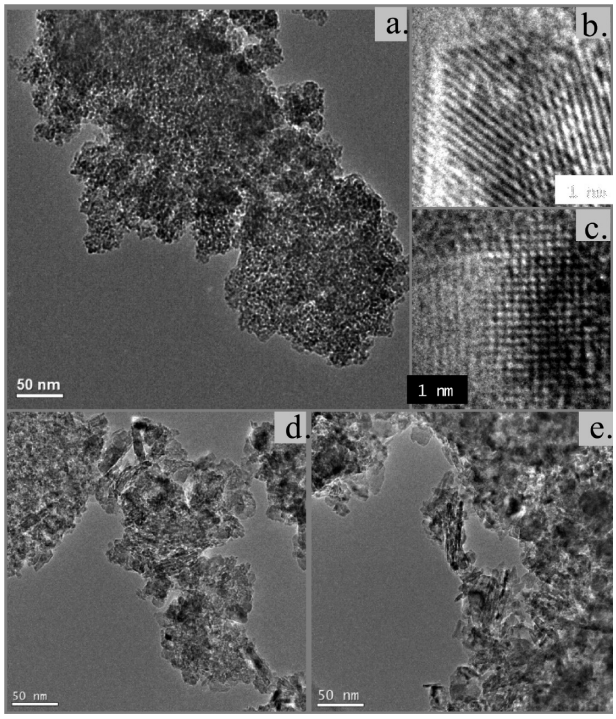

Figure 5. TEM micrographs of samples calcined at 550 °C: (a) MgAl-E, (b) HRTEM of MgAl-E, showing Mg(Al)O phase, (c) HRTEM of MgAl-E, showing nanocrystalline γ-Al_2O_3, (d) MgAl-TH1W, and (e) MgAl-CP.

sheets. The broadness of the peak varied significantly for the various samples, Table 2. The narrowest peak was found for the sample MgAl-TH1W, and the broadest one was for the sample MgAl-E. Besides, the spectrum of sample MgAl-TH10 was the only one that presented a low intensity peak at 71 ppm, which is assigned to tetrahedral aluminum.

After treatment at 250 °C, ^{27}Al MAS NMR spectra (Figure 8) were mainly composed by the resonance of octahedral aluminum (Al^{VI}), but the signal due to tetrahedral aluminum (Al^{IV}) is also evident in all cases. At this temperature, MgAl-E presented the most intense signal of Al^{IV}.

Thermal treatment at 550 °C induces modifications in the environment of aluminum ions. Spectra in Figure 9 show a decreasing intensity of the octahedral resonance, due to the apparition of an intense resonance of Al^{IV}. All of the calcined samples exhibited similar ^{27}Al NMR spectra; qualitatively, they all have the same relative amounts of Al^{VI} and Al^{IV}.

When the samples recover the layered structure by rehydration, the local environment of aluminum is not exactly the same as in the fresh samples, as shown by the ^{27}Al NMR spectra in Figure 10. For instance, in samples MgAl-E and MgAl-TH1W, a residual amount of tetrahedral aluminum produced upon calcination has not recuperated its octahedral coordination. On the contrary, as-synthesized sample MgAl-TH10 exhibited tetrahedral aluminum, but after calcination−rehydration only octahedral aluminum is detected. Furthermore, the resonance peak of octahedral aluminum is significantly narrower after the calcination−rehydration cycle, Table 2.

^{13}C CP MAS NMR spectra of fresh samples MgAl-E and MgAl-TH10, Figure 11, revealed that acetate groups (signals at 24.5 and 179.6 ppm assigned to methyl and carbonyl, respectively) are present as charge-compensating anions. The signal at 51.9 ppm is due to −CH−O from alkoxide species also intercalated between the brucite-like layers. The bands due to acetate are significantly more intense for MgAl-E than for

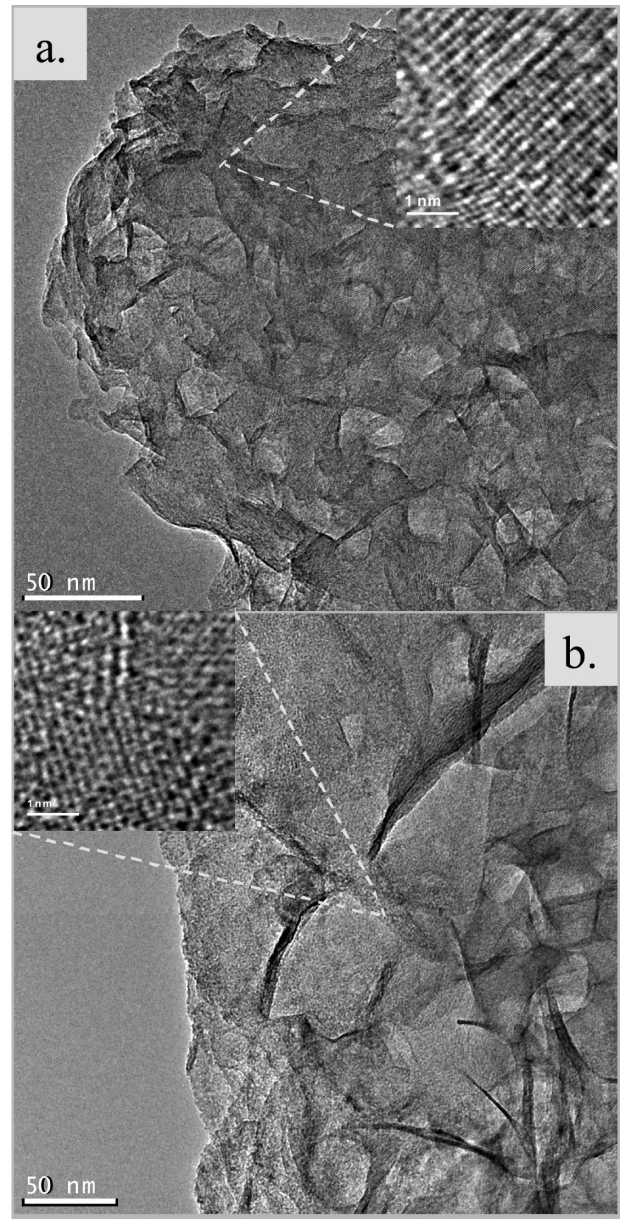

Figure 6. TEM micrographs of calcined (550 °C) and rehydrated samples: (a) MgAl-E and (b) MgAl-CP.

MgAl-TH10; conversely, the alkoxide peak is more intense in MgAl-TH10. Therefore, acetates were replaced by ethoxy anions during hydrothermal treatment. Last, the signal at 169 ppm corresponds to carbonate anions. With calcination at temperature as high as 550 °C, these organic species were removed. However, when rehydrated samples recover the layered structure, they incorporate carbonate species to compensate the positive charge of brucite-like-layers, Figure 11c.

3.4. X-ray Photoelectron Spectroscopy. Al 2p XPS spectra of all fresh samples showed a single peak with binding energy (BE) centered at 74.0 ± 0.1 eV corresponding to octahedral Al^{3+} in an LDH structure. The Mg 2p spectra showed also a single peak occurring at 49.6 ± 0.1 eV, characteristic of Mg^{2+} in an LDH phase. For sample MgAl-TH10, both BE values shifted slightly; see Table 3. Concerning O 1s XPS spectra, it presented two peaks with main positions at 531.0−531.6 and 528.0−529.0 eV. The first one, with very high intensity, is attributed to the oxygen species in LDH structure, whereas the low intensity second peak corresponds to oxygen bonded to

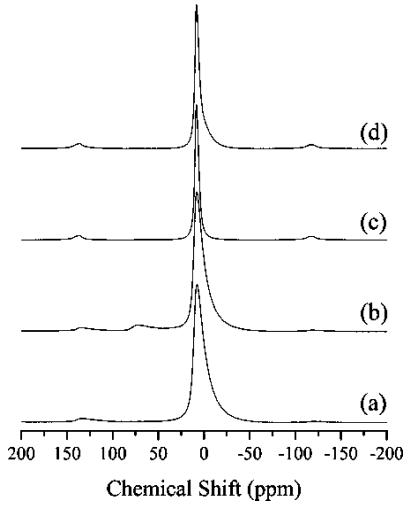

Figure 7. ^{27}Al MAS NMR spectra of as-synthesized samples: (a) MgAl-E, (b) MgAl-TH10, (c) MgAl-TH1W, and (d) MgAl-CP.

TABLE 2: Line Width (Hz) of ^{27}Al NMR Signal at 5 ppm (Octahedral Aluminum)

sample	as-synthesized	treated at 250 °C	calcined−rehydrated
MgAl-E	1036	1052	763
MgAl-TH10	1006	913	407
MgAl-TH1W	459	1021	814
MgAl-CP	528	1090	549

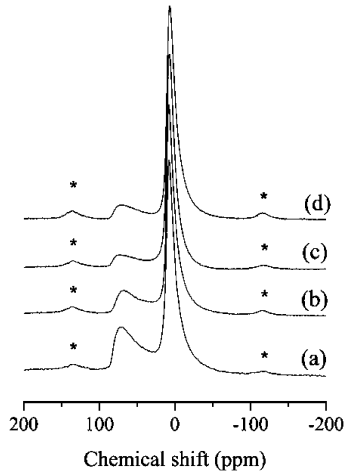

Figure 8. ^{27}Al MAS NMR spectra of samples after thermal treatment at 250 °C: (a) MgAl-E, (b) MgAl-TH10, (c) MgAl-TH1W, and (d) MgAl-CP. "*" indicates spinning side bands (spinning rate of 10 kHz).

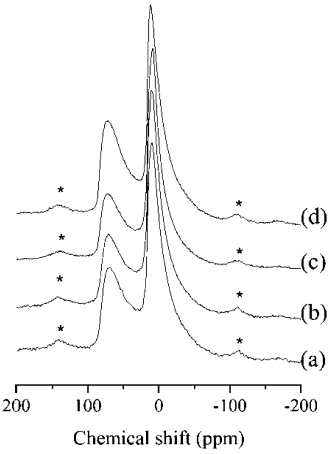

Figure 9. ^{27}Al MAS NMR spectra of samples calcined at 550 °C: (a) MgAl-E, (b) MgAl-TH10, (c) MgAl-TH1W, and (d) MgAl-CP. "*" indicates spinning side bands (spinning rate of 10 kHz).

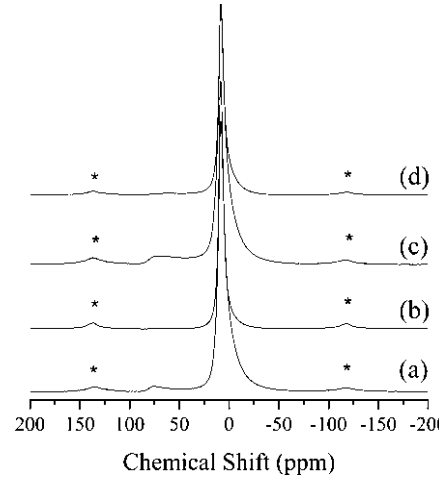

Figure 10. ^{27}Al MAS NMR spectra of calcined (550 °C) and rehydrated samples: (a) MgAl-E, (b) MgAl-TH10, (c) MgAl-TH1W, and (d) MgAl-CP. "*" indicates spinning side bands (10 kHz).

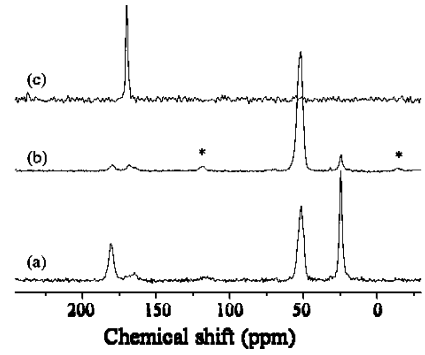

Figure 11. ^{13}C CP MAS NMR spectra of samples: (a) as-synthesized MgAl-E, (b) as-synthesized MgAl-TH10, and (c) calcined (550 °C) and rehydrated MgAl-TH10. "*" indicates spinning side bands (10 kHz).

carbon species in the interlayer position of LDH structure (results not shown).

On all of the calcined samples (550 °C), the Al 2p signal was adjusted by using two components, both with the same fwhm (Figure 12). The first one, occurring around 74.5 eV, is assigned to octahedrally coordinated Al^{3+}, whereas the second one, occurring around 73.5 eV, must be assigned to tetrahedrally coordinated Al^{3+}.[38] Only in the sample MgAl-E was a less intense third peak observed at lower binding energy. This peak could be attributed to strongly deformed Al species that were created by the curved structure of the particular nanocapsular morphology shown by the as-synthesized sample.

Samples hydrothermally treated in alcohol or alcohol/water mixture, MgAl-TH10 and MgAl-TH1W, respectively, showed a more intense tetrahedral Al peak than the sample obtained by coprecipitation. The $Al^{IV}/(Al^{VI} + Al^{VI})$ atomic ratios are shown in Table 4. Samples that were subjected to hydrothermal treatment expose higher amounts of Al^{IV} on its surface after calcination. In fact, around 35% of Al atoms exposed at the surface present tetrahedral coordination, whereas in samples not hydrothermally treated, MgAl-E and MgAl-CP, there is only ~20% of Al^{IV} at the surface.

Figure 13 shows the Mg 2p XP spectra of calcined samples, which were also adjusted by two components. The first one,

TABLE 3: XPS Binding Energy Values and Assignment for As-Synthesized, Calcined (550 °C), and Rehydrated Samples[a]

sample	treatment	binding energy Al 2p (eV)	assignment	binding energy Mg 2p (eV)	assignment
MgAl-E	as-synthesized	74.1	Al^{VI} in LDH	49.7	Mg in LDH
		74.7	Al^{VI} in MO	50.3	Mg in MO
	calcined (550 °C)	72.2	Al^{IV} in MO	48.5	Mg in MgO
		69.6	Al defect		
	calcined and rehydrated	75.6	Al^{VI} in MO	51.2	Mg in MO
		74.1	Al^{VI} in LDH	49.6	Mg in LDH
MgAl-TH10	as-synthesized	73.6	Al^{VI} in LDH	49.3	Mg in LDH
	calcined (550 °C)	75.0	Al^{VI} in MO	50.9	Mg in MO
		73.1	Al^{IV} in MO	48.9	Mg in MgO
	calcined and rehydrated	74.3	Al^{VI} in MO	50.9	Mg in MO
		73.7	Al^{VI} in LDH	49.5	Mg in LDH
MgAl-TH1W	as-synthesized	74.0	Al^{VI} in LDH	49.6	Mg in LDH
	calcined (550 °C)	74.8	Al^{VI} in MO	50.5	Mg in MO
		73.3	Al^{IV} in MO	49.1	Mg in MgO
	calcined and rehydrated	74.8	Al^{VI} in MO	50.5	Mg in MO
		73.8	Al^{VI} in LDH	49.4	Mg in LDH
MgAl-CP	as-synthesized	73.9	Al^{VI} in LDH	49.6	Mg in LDH
	calcined (550 °C)	74.2	Al^{VI} in MO	50.1	Mg in MO
		72.6	Al^{IV} in MO	48.7	Mg in MgO
	calcined and rehydrated	74.9	Al^{VI} in MO	51.0	Mg in MO
		74.0	Al^{VI} in LDH	49.6	Mg in LDH

[a] MO = mixed oxide, Al^{IV} = tetrahedral aluminum, Al^{VI} = octahedral aluminum.

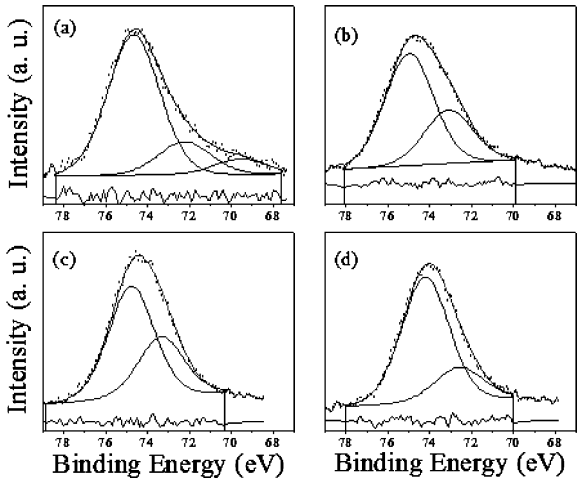

Figure 12. XPS spectra of the Al 2p region for quasi in situ calcined (550 °C) samples: (a) MgAl-E, (b) MgAl-TH10, (c) MgAl-TH1W, and (d) MgAl-CP.

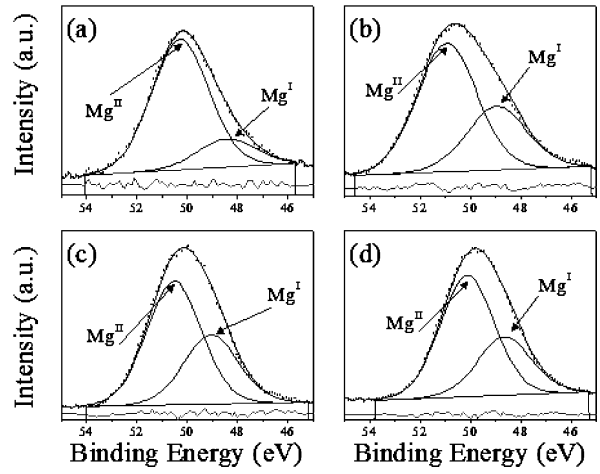

Figure 13. XPS spectra of the Mg 2p region for quasi in situ calcined (550 °C) samples: (a) MgAl-E, (b) MgAl-TH10, (c) MgAl-TH1W, and (d) MgAl-CP.

denoted as Mg^{I}, is located around 48.8 eV and must be assigned to Mg^{2+} in periclase MgO structure.[39] The second one, marked as Mg^{II} in Figure 13, centered on 50.4 eV corresponds to Mg^{2+} in strong interaction with Al atoms, in Mg−O−Al bonds. It is interesting to remark that the evolution of Mg^{2+} in MgO periclase structure closely corresponds to the amount of Al^{3+}

TABLE 4: Atomic Ratios Determined from XPS Parameters

		atomic ratios[a]				
sample	treatment	Mg/Al	$Al^{IV}/(Al^{IV} + Al^{VI})$	$Mg^{I}/(Mg^{I} + Mg^{II})$	$Al_{LDH}{}^{VI}/(Al_{LDH}{}^{VI} + Al^{VI}{}_{MO})$	$Mg_{LDH}/(Mg_{LDH} + Mg_{MO})$
MgAl-E	as-synthesized	2.5			1.0	1.0
	calcined	2.5	0.19	0.18		
	rehydrated	3.5			0.86	0.87
MgAl-TH10	as-synthesized	3.2			1.0	1.0
	calcined	3.2	0.32	0.33		
	rehydrated	3.4			0.58	0.93
MgAl-TH1W	as-synthesized	3.5			1.0	1.0
	calcined	3.1	0.35	0.36		
	rehydrated	3.5			0.55	0.57
MgAl-CP	as-synthesized	3.2			1.0	1.0
	calcined	3.7	0.21	0.32		
	rehydrated	2.4			0.84	0.90

[a] MO = mixed oxide, Al^{IV} = tetrahedral aluminum, Al^{VI} = octahedral aluminum.

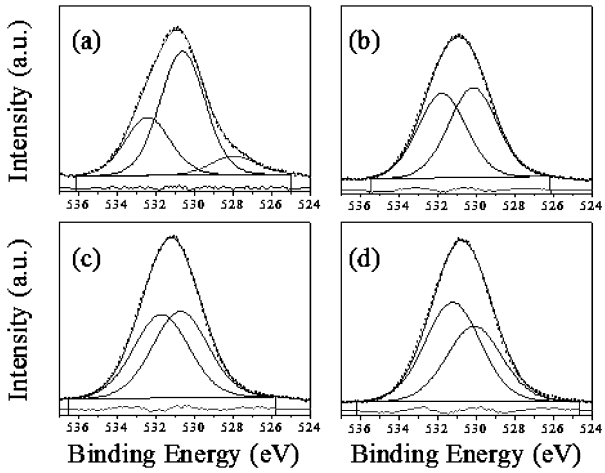

Figure 14. XPS spectra of the O 1s region for quasi in situ calcined (550 °C) samples: (a) MgAl-E, (b) MgAl-TH10, (c) MgAl-TH1W, and (d) MgAl-CP.

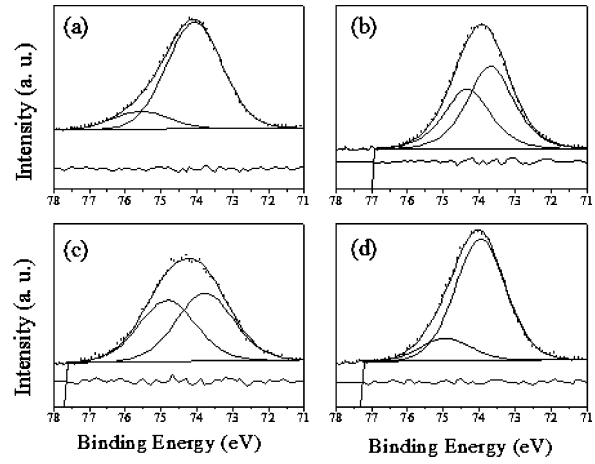

Figure 15. XPS spectra of the Al 2p region for calcined (550 °C) and rehydrated samples: (a) MgAl-E, (b) MgAl-TH10, (c) MgAl-TH1W, and (d) MgAl-CP.

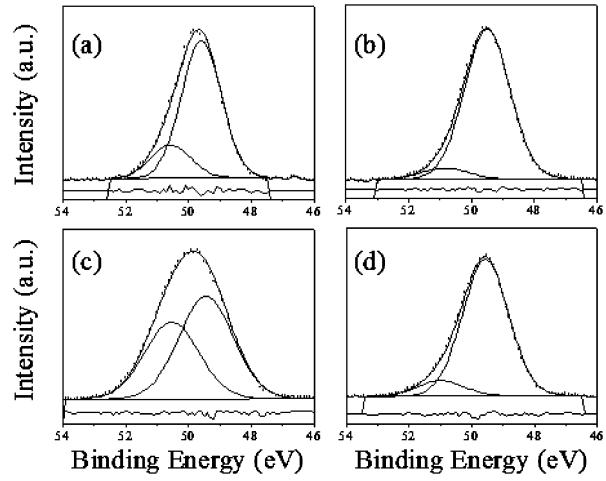

Figure 16. XPS spectra of the Mg 2p region for calcined (550 °C) and rehydrated samples: (a) MgAl-E, (b) MgAl-TH10, (c) MgAl-TH1W, and (d) MgAl-CP.

in tetrahedral coordination (Table 4). Only in the sample MgAl-CP, obtained by conventional coprecipitation, does the amount of Al^{3+} in tetrahedral coordination differ from the surface amount of Mg^{2+} segregated as MgO; however, the results indicate a similar trend.

XPS O 1s spectra of calcined samples are presented in Figure 14. The O 1s spectra were deconvoluted by using two oxygen components, except for the MgAl-E sample, in which a low intensity third peak at 528.0 eV was necessary for a correct fit of the spectrum. This O 1s peak can be attributed to oxygen atoms carrying a higher negative charge, very likely surface atoms with a low coordination number that may be found in surface crystalline defects. For the other O 1s signals, the first one occurred at 531.2−531.8 eV, and its intensity increased as the LDH precursor crystallite size decreased. The second O 1s peak occurred at 530.1−530.7 eV; in this case, its intensity decreased with the crystallite size. According to the literature, a single component for the O 1s XPS spectrum at 530.9 eV has been reported for pure alumina attributed to the hydroxylated oxygen species at the alumina surface,[40] whereas for the pure MgO periclase phase two O 1s components have been found at 530.9 and 529.3 eV, the first one attributed to the parent state of Me−O−Me oxygen species, and the second one at lower BE is characteristic of basic O^{2-} surface species.[41] When Mg is incorporated in an LDH structure, a shift of the O 1s BE position is expected; then, the peak observed at 530.1−530.7 eV must correspond to the basic O^{2-} species, whereas that occurring at higher BE, around 531.2−531.8 eV, can be attributed to strongly bonded oxygen species in Mg−O−Al surface bonds.

The XPS Al 2p signals for the rehydrated samples are shown in Figure 15. As it can be seen in all samples, the Al 2p spectra were fitted by using two components at BE values of 73.7−74.0 and 74.3−74.9 eV. The first one occurs nearly at the same BE value of the as-synthesized LDH and must correspond to Al^{3+} in octahedral coordination that returned to the LDH structure, whereas the second one, at higher BE value, must correspond to Al^{3+} atoms also in octahedral coordination but with a different electronic environment. As compared to the calcined samples, these Al atoms correspond to those octahedrally coordinated in the alumina phase or those in strong interaction with Mg atoms forming Mg−O−Al bonds. The Al^{IV} atoms observed after calcination at BE values lower than 73.3 eV disappeared completely after rehydration. MgAl-CP sample showed a similar behavior, as not all of the surface Al atoms were restored to the LDH structure, although a higher fraction of the Al atoms get back to the BE value of the as-synthesized LDH. The proportion of surface Al atoms restoring to the LDH structure was estimated by the $Al^{VI}_{LDH}/(Al^{VI}_{MO} + Al^{VI}_{LDH})$ atomic ratio presented in Table 4. In samples MgAl-TH10 and MgAl-TH1W, subjected to hydrothermal treatment, only 55−58% of Al atoms restore the LDH structure, whereas in samples MgAl-E and MgAl-CP, 84−86% of Al atoms restore the LDH phase.

The Mg 2p spectra of rehydrated samples are shown in Figure 16. All spectra were deconvoluted with two components. The first one occurs at the same BE value of LDH phase, around 49.6 eV, and corresponds to Mg^{2+} atoms in LDH structure. The second one, occurring at higher BE, around 50.7 eV, must correspond to Mg atoms in strong interaction with Al atoms in the mixed oxide producing Mg−O−Al bonds. The peak at around 48.6 eV, characteristic of Mg^{2+} in the periclase MgO phase, completely disappeared, suggesting that all Mg^{2+} reincorporates to the LDH phase. As for the Al 2p signal, the proportion of Mg atoms restoring the LDH structure was estimated by the $Mg_{LDH}/(Mg_{LDH} + Mg_{MO})$ atomic ratio presented in Table 4. Similarly to the Al 2p signal, in MgAl-TH1W a larger amount of Mg atoms did not restore the LDH structure. In fact, the proportion of Mg that restored to the LDH phase nearly corresponds to that of Al atoms in this sample, supporting

the hypothesis that these Mg atoms remain in strong interaction with Al atoms, and that these surface Mg−O−Al bonds are responsible for the low restoring capacity of MgAl-TH10 and MgAl-TH1W, suggesting that stronger Mg−O−Al bonds are obtained when sol−gel LDHs precursors are submitted to hydrothermal treatment.

After rehydration, the XPS O 1s signal showed a single peak with a position at 531.5 eV characteristic of the hydroxylated oxygen species,[42] nearly at the same position of O 1s of as-synthesized LDH samples, suggesting that all surface oxygen atoms were rehydrated (data not shown).

4. Discussion

Previous studies on these materials revealed that the peculiar nanocapsular morphology of sol−gel samples is restricted to nonaqueous media; it was proposed that the curvature of LDH layers and the formation of the nanocapsules are driven by the hydrophobicity of the alcohol's organic tail.[12] During hydrothermal treatment in the mother liquor (ethanol), the capsules have been observed to coalesce; crystallinity also increases during this treatment.[12] This crystallization process is related to the reactions that take place during a sol−gel synthetic process, mainly hydrolysis, condensation, and polymerization.[43] Acetic acid is introduced during synthesis to hinder hydrolysis and condensation of the aluminum alkoxide; this enables the equalization of reaction rates between magnesium and aluminum, and thus the formation of a pure LDH phase.[11] Acetate groups are very likely acting as a bidentate chelating ligand, based on the separation (Δ) between the antisymmetric and symmetric stretching vibrations of the carboxyl groups observed by FTIR (data not shown).[44,45] These groups are less reactive than alkoxides,[46] so they remain in the LDH structure as the main charge-compensating anions, as observed by the ^{13}C NMR of as-synthesized MgAl-E (Figure 11). During hydrothermal treatment with ethanol as solvent, condensation reactions are accelerated by temperature, and acetate groups are replaced by alkoxides in sample MgAl-TH10. This is confirmed both by ^{13}C NMR spectra (Figure 10) and by the increased crystallinity observed by XRD (Figure 1 and Table 1). Also in support of this hypothesis are the interlayer distances of MgAl-E and MgAl-TH10, which are very similar among them, as acetate and ethoxy molecules have very similar sizes, and much larger than those of MgAl-TH1W and MgAl-CP (Figure 1 and Table 1).

In MgAl-E, acetate acting as a bidentate chelating ligand occupies two coordination spaces of the aluminum center,[44] leading to octahedral species with a strong electric field gradient, which broadens the resonance peak (see Figure 7 and Table 2). When acetate is replaced by a monodentate molecule such as alkoxide, the coordination is lowered, and tetrahedral aluminum appears in the NMR spectra of as-synthesized MgAl-TH10. These Al^{IV} species are metastable; in fact, they are unable to reach their natural octahedral coordination because of the substoichiometric amount of water that was introduced.[11] It is worth noting that the Al 2p XPS spectra of as-synthesized MgAl-TH10 did not present a peak at lower binding energy that could be ascribed to tetrahedral aluminum. Therefore, these Al^{IV} species are not at the surface of the material; they must be located in the layers that are nearer to the core of the nanocapsule. Very likely, surface aluminum atoms are the first to react and thus are able to achieve octahedral coordination.

The large amounts of acetate in MgAl-E also explain why this sample presents more tetrahedral aluminum at 250 °C. A small fraction of octahedral Al in an LDH are expected to migrate and adopt tetrahedral coordination when temperature is increased above 200 °C.[26] In agreement with this, some Al^{IV} was observed on the ^{27}Al NMR spectra of samples heated at 250 °C (Figure 8). In sample MgAl-E, additional tetrahedral aluminum appears because of the removal of acetate by thermal decomposition. To a lesser extent, this also occurs in MgAl-TH10, which still had some residual acetate. Therefore, the amount of tetrahedral aluminum at 250 °C is MgAl-E > MgAl-TH10 > MgAl-TH1W $\approx$ MgAl-CP.

In sample MgAl-TH1W, two factors intervene that explain why it is more like a coprecipitated sample, even though its synthesis procedure is the same as in MgAl-E and MgAl-TH10. First, the addition of excess (50% vol.) water during hydrothermal treatment neutralizes the strong hydrophobic interactions between R groups and favors the formation of platelets. Furthermore, water significantly accelerates hydrolysis reactions; hydrolyzed species in turn condense more rapidly.[43] Therefore, a highly crystalline LDH is obtained; the tetrahedral aluminum species created when acetate is removed continue to react until they reach octahedral coordination. The second factor is that no special precautions were taken to avoid carbonate contamination (for example, decarbonated water, inert atmosphere, etc.). Acetate and alkoxy groups are replaced by carbonate, given the well-known affinity of LDHs for this molecule.[1,2] Thus, MgAl-TH1W and MgAl-CP have nearly the same interlayer distance (Figure 1 and Table 1).

Comparing the Mg/Al molar ratios of the as-synthesized samples obtained by ICP (Table 1) with the Mg/Al atomic ratios determined by XPS (Table 4), it appears that the surface is deficient in aluminum. In sample MgAl-E, there apparently is no difference between surface (XPS) and bulk (ICP) compositions, but this is due to the very small nanocapsules of this sample, which range from 10 to 40 nm. The depth analyzed by XPS, 10−50 Å, is actually all of the capsule's shell, that is, all of the layers that compose the particle.

When samples are treated at temperatures as high as 550 °C, the alkoxy and acetate anions are completely removed, the layered structure collapses, and the periclase-like structure is formed in all samples. Crystal sizes of the Mg(Al)O mixed oxide obtained by calcination are affected by the crystallinity of the as-synthesized sample (Table 1). The tendency of crystal sizes, MgAl-TH1W > MgAl-CP > MgAlTH10 > MgAl-E, is maintained, although the differences are not as significant in the calcined as in the as-synthesized samples. Morphology after calcination is closely related to the morphology of the as-synthesized samples. Nanocapsules become an agglomeration of globular nanoparticles, while platelets create a disordered house-of-cards structure. Previously, these calcined samples were analyzed by N_2 physisorption;[12] the differences in hysteresis loops correspond to the different morphologies observed by TEM.

Tetrahedral aluminum in the bulk of the calcined samples, measured by ^{27}Al MAS NMR (Figure 9), shows that there is a similar proportion of Al^{IV} in all samples, despite the fact that at 250 °C there was clearly more Al^{IV} in MgAl-E and MgAl-TH10. It appears that there is a maximum amount of aluminum that can migrate to tetrahedral positions, without affecting the formation of the mixed oxide. Therefore, Al^{IV} population may be an inherent property of calcined LDHs, dependent only on calcination conditions and not on anions, morphology, or crystal size of the as-synthesized LDH.

However, the location of these Al^{IV} species varies considerably with the synthesis procedure. For sample MgAl-E, XPS detected ~20% Al^{IV}. Here, again, the depth analyzed by XPS

is indeed the whole particle, so no significant differences are appreciated between surface and bulk compositions. However, comparisons between samples of large crystal sizes, samples MgAl-TH1W and MgAl-CP, show a significant difference in surface tetrahedral aluminum, 35% and 21%, respectively (Table 4). MgAl-TH10 also has ~30% of surface Al^{IV}. Thus, the sol−gel synthesis procedure apparently favors the migration of Al^{IV} species to the surface. It is possible that the sol−gel method, because of its soft synthesis conditions, enhances the creation of defects in the crystal lattice, which facilitates the migration of cations. In fact, in MgAl-TH1W, there occurs an enrichment of aluminum at the surface, evidenced by the decrease in Mg/Al atomic ratio measured by XPS, from 3.5 to 3.1 (Table 4). On the contrary, MgAl-CP presents a surface enrichment of Mg, as seen by the increase from 3.2 to 3.7 of the Mg/Al atomic ratio.

Another important difference between the sol−gel and the coprecipitated samples appears in the O 1s XP spectra of the calcined samples, Figure 14. Coluccia and Tench proposed a model for the generation of basic sites in a MgO crystal, which states that there are a number of Mg−O pairs with different coordination number.[47,48] Ion pairs of low coordination exist at crystal defects such as corners and edges. As crystals become smaller, there is a higher amount of crystal defects, and consequently higher amounts of O^{2-} species. This hypothesis is supported by the intensity of the peak at lower binding energy (~530 eV) in the O 1s spectra of calcined samples. This peak, corresponding to O^{2-} species, is more intense in sol−gel than in coprecipitated calcined LDHs, particularly in MgAl-E. This sample has also a third peak at lower binding energy (528 eV), which may be ascribed to oxygen atoms with very low coordination and high negative charge.

During rehydration, several processes take place. First, all samples presented a disordered stacking of platelets, creating a house-of-cards structure, independently of the initial morphology (Figure 6). This is probably due to the fact that the nanocapsular morphology of the as-synthesized MgAl-E and MgAl-TH10 is metastable. Slow reconstruction under ambient moisture leads to the formation of the traditional, more stable, platelet morphology. However, a few semispherical voids were observed by TEM, remnant of the initial nanocapsules.

Crystal sizes of the rehydrated samples (Table 1) present a tendency drastically different from that of the as-synthesized samples. Samples MgAl-TH1W and MgAl-CP, which originally had the largest crystals, show a decrease in crystallinity. This is consistent with previous reports, which state that during the calcination−reconstruction process there is a loss of crystallinity. However, in samples MgAl-E and MgAl-TH10, crystal sizes increased, contradicting previous reports. Given these data, it may be concluded that crystallinity in the reconstructed LDH depends on the reconstruction procedure, time, temperature, etc., but not on the crystal sizes of the original LDH, as is commonly thought.[22] This phenomenon is only observed clearly when LDHs with very small crystals are used. Samples with such reduced crystallinity would be very hard to synthesize by procedures other than the sol−gel method; this explains why it has remained hitherto unseen.

Sol−gel samples present a surface enrichment of magnesium, based on the increase in Mg/Al atomic ratio measured by XPS (Table 4). This migration of aluminum cations from the surface to the bulk of the materials is more significant for samples MgAl-E and MgAl-TH1W. These two samples also presented some residual Al^{IV} species that were only detected by NMR (Figure 10). Probably, migration of Al^{IV} to the bulk causes the restoring process to be slower in these samples, so that after 10 days they have not attained their full coordination. It is important to bear in mind that rehydration was performed by placing the samples in a moist environment. There was no direct contact with an aqueous solution, nor was there a flow of water-saturated nitrogen going through the samples, as rehydration is usually done. Therefore, reconstruction of the layered structure is expected to be slower. Furthermore, the samples were not filtered or washed after reconstruction, as this could alter the samples' composition.

It is reported that all aluminum atoms recover their octahedral coordination if sufficient time is given.[24] The amount of time that will be sufficient depends on several factors, such as calcination temperature, rehydration procedure, and original interlayer anions.

Sample MgAl-TH10 does not have any Al^{IV} after rehydration, and migration of aluminum is less significant (Mg/Al ratio changed from 3.2 to 3.4). However, it is interesting that, in this case, the fraction of aluminum that does not return to the LDH structure is very significant, while 93% of magnesium recovers LDH phase. This tendency is probably maintained in the bulk; this causes the increase in the *a* unit cell parameter observed by XRD, which indicates that the rehydrated LDH phase contains less aluminum than the as-synthesized sample (Table 1).

Sample MgAl-CP has an entirely different behavior; it shows the most important variation in Mg/Al surface atomic ratio, from 3.7 (calcined) to 2.4 (rehydrated), in contrast to the behavior shown by MgAl-E sample, in which the Mg/Al surface atomic ratio increased from 2.5 to 3.5 for calcined and rehydrated samples respectively. These results can be explained by the opposite behavior of crystallite size of fresh and rehydrated conditions in both samples. Even though aluminum migration occurs in every case, in smaller crystals it should be easier for these cations to reach the surface.

5. Conclusions

The evolution of crystallinity and morphology in LDHs with different synthesis procedures (sol−gel and coprecipitation) and different postsynthesis treatments was studied throughout the calcination−reconstruction process by XRD and TEM. It was observed that, regardless of initial morphology, all samples reconstruct into the more stable platelet-like morphology that is traditional of LDHs. Also, it was found that, contrary to what is believed, crystal sizes do not necessarily decrease from the as-synthesized to the reconstructed LDH. In fact, crystallinity depends mostly on the reconstruction conditions. Furthermore, the migration of aluminum from octahedral to tetrahedral coordination was monitored by ^{27}Al MAS NMR and by XPS; the structural environment of surface magnesium and oxygen species was also analyzed by XPS. Tetrahedral aluminum was detected in an as-synthesized, sol−gel LDH; this unusual formation of Al^{IV} was explained in terms of the basic sol−gel reactions that take place during synthesis and crystallization. Formation of Al^{IV} was initially faster in sol−gel samples, but after calcination at 550 °C its population is essentially the same, regardless of the preparation procedure. It can be concluded that there is a maximum amount of Al^{IV} species that can be created without altering the formation of the Mg(Al)O phase characteristic of calcined LDHs, and that the population of Al^{IV} depends mostly on the calcination temperature. However, the population of Al^{IV} at the surface is higher in sol−gel samples, indicating an increased migration of these cations, probably because of the formation of more structural defects during

sol−gel synthesis. Additionally, XPS detected magnesium in two different structural environments. Calcined LDHs had Mg interacting with aluminum forming a Mg(Al)O mixed oxide, plus Mg in, apparently, pure MgO periclase-like structure. The relative population of these Mg species is closely correlated to the percentage of Al^{IV}. After reconstruction, most magnesium returns to the LDH phase, but a small fraction remains in strong interaction with aluminum, forming a nonstoichiometric magnesium−aluminum oxide.

Acknowledgment. We thank the Mexican Institute of Petroleum for financial support and Dr. M. E. Llanos for facilitating access to XPS equipment. J.P. gratefully acknowledges CONACyT for a graduate school scholarship.

References and Notes

(1) Cavani, F.; Trifiro, F.; Vaccari, A. *Catal. Today* **1991**, *11*, 173.
(2) Rives, V., Ed. *Layered Double Hydroxides: Present and Future*; Nova Science Publishers, Inc.: New York, 2001.
(3) Duan, X., Evans, D. G., Eds. Layered Double Hydroxides. *Structure and Bonding*; Springer-Verlag: Berlin Heidelberg, Germany, 2006; Vol. 119.
(4) Figueras, F. *Top. Catal.* **2004**, *29*, 189.
(5) Valente, J. S.; Lopez-Salinas, E.; Cantu, M. S.; Hernandez-Beltran, F. U.S. Patent 2006/0189481 A1, 2006.
(6) Climent, M. J.; Corma, A.; Iborra, S.; Epping, K.; Velty, A. *J. Catal.* **2004**, *225*, 316.
(7) Benito, P.; Labajos, F. M.; Rives, V. *Cryst. Growth Des.* **2006**, *6*, 1961.
(8) Benito, P.; Herrero, M.; Barriga, C.; Labajos, F. M.; Rives, V. *Inorg. Chem.* **2008**, *47*, 5453.
(9) Lopez, T.; Bosch, P.; Ramos, E.; Gomez, R.; Novaro, O.; Acosta, D.; Figueras, F. *Langmuir* **1996**, *12*, 189.
(10) Prinetto, F.; Ghiotti, G.; Graffin, P.; Tichit, D. *Microporous Mesoporous Mater.* **2000**, *39*, 229.
(11) Valente, J. S.; Cantu, M. S.; Cortez, J. G. H.; Montiel, R.; Bokhimi, X.; Lopez-Salinas, E. *J. Phys. Chem. C* **2007**, *111*, 642.
(12) Valente, J. S.; Prince, J.; Maubert, A. M.; Lartundo-Rojas, L.; Angel, P.; Ferrat, G.; Hernandez, J. G.; Lopez-Salinas, E. *J. Phys. Chem. C* **2009**, *113*, 5547.
(13) Wang, D.-Y.; Costa, F. R.; Vyalikh, A.; Leuteritz, A.; Scheler, U.; Jehnichen, D.; Wagenknecht, U.; Haussler, L.; Heinrich, G. *Chem. Mater.* **2009**, *21*, 4490.
(14) Valente, J. S.; Figueras, F.; Gravelle, M.; Kumbhar, P.; Lopez, J.; Besse, J.-P. *J. Catal.* **2000**, *189*, 370.
(15) Kumbhar, P. S.; Sanchez-Valente, J.; Lopez, J.; Figueras, F. *Chem. Commun.* **1998**, 535.
(16) Valente, J. S.; Tzompantzi, F.; Prince, J.; Cortez, J. G. H.; Gomez, R. *Appl. Catal., B* **2009**, *90*, 330.
(17) Cantu, M.; Lopez-Salinas, E.; Valente, J. S.; Montiel, R. *Environ. Sci. Technol.* **2005**, *39*, 9715.
(18) Rao, K. K.; Gravelle, M.; Valente, J. S.; Figueras, F. *J. Catal.* **1998**, *173*, 115.
(19) Kumbhar, P. S.; Valente, J. S.; Figueras, F. *Chem. Commun.* **1998**, 1091.
(20) Prinetto, F.; Ghiotti, G.; Durand, R.; Tichit, D. *J. Phys. Chem. B* **2000**, *104*, 11117.
(21) Climent, M. J.; Corma, A.; Iborra, S.; Velty, A. *J. Catal.* **2004**, *221*, 474.
(22) Hibino, T.; Tsunashima, A. *Chem. Mater.* **1998**, *10*, 4055.
(23) van Bokhoven, J. A.; Roelofs, J. C. A. A.; de Jong, K. P.; Koningsberger, D. C. *Chem.-Eur. J.* **2001**, *7*, 1258.
(24) Roelofs, J. C. A. A.; Lensveld, D. J.; van Dillen, A. J.; de Jong, K. P. *J. Catal.* **2001**, *203*, 184.
(25) Roelofs, J. C. A. A.; van Bokhoven, J. A.; van Dillen, A. J.; Geus, J. W.; de Jong, K. P. *Chem.-Eur. J.* **2002**, *8*, 5571.
(26) Bellotto, M.; Rebours, B.; Clause, O.; Lynch, J.; Bazin, D.; Elkaïm, E. *J. Phys. Chem.* **1996**, *100*, 8535.
(27) Yang, W.; Kim, Y.; Liu, P. K. T.; Sahimi, M.; Tsotsis, T. T. *Chem. Eng. Sci.* **2002**, *57*, 2945.
(28) Kanezaki, E. *Solid State Ionics* **1998**, *106*, 279.
(29) Winter, F.; Xia, X.; Hereijgers, B. P. C.; Bitter, J. H.; van Dillen, A. J.; Muhler, M.; de Jong, K. P. *J. Phys. Chem. B* **2006**, *110*, 9211.
(30) Chimentão, R. J.; Abelló, S.; Medina, F.; Llorca, J.; Sueiras, J. E.; Cesteros, Y.; Salagre, P. *J. Catal.* **2007**, *252*, 249.
(31) Millange, F.; Walton, R. I.; O'Hare, D. *J. Mater. Chem.* **2000**, *10*, 1713.
(32) Rebours, B.; d'Espinose de la Caillerie, J. B.; Clause, O. *J. Am. Chem. Soc.* **1994**, *116*, 1707.
(33) Puttaswamy, N. S.; Kamath, P. V. *J. Mater. Chem.* **1997**, *7*, 1941.
(34) Stanimirova, T.; Hibino, T.; Balek, V. *J. Therm. Anal. Calorim.* **2006**, *84*, 473.
(35) *Thermo VG-Scientific. XPS and Auger Handbook*; Doc. Number: 600001 issue 2, 2003.
(36) Pausch, I.; Lohse, H. H.; Schürmann, K.; Allmann, R. *Clays Clay Miner.* **1986**, *34*, 507.
(37) Gursky, J. A.; Blough, S. D.; Luna, C.; Gomez, C.; Luevano, A. N.; Gardner, E. A. *J. Am. Chem. Soc.* **2006**, *128*, 8376.
(38) Rao, M. M.; Reddy, B. R.; Jayalakshmi, M.; Jaya, V. S.; Sridhar, B. *Mater. Res. Bull.* **2005**, *40*, 347.
(39) Cantrell, D. G.; Guillie, L. J.; Lee, A. F.; Wilson, K. *Appl. Catal., A* **2005**, *287*, 183.
(40) Albuquerque, M. C. G.; Santamaría-González, J.; Mérida-Robles, J. M.; Moreno-Tost, R.; Rodríguez-Castellón, E.; Jiménez-López, A.; Azevedo, D. C. S.; Cavalcante, C. L., Jr.; Maireles-Torres, P. *Appl. Catal., A* **2008**, *162*, 347.
(41) Peng, X. D.; Richards, D. A.; Stair, P. C. *J. Catal.* **1990**, *121*, 99.
(42) Barr, T. L.; Seal, S.; Wozniak, K.; Klinowski, J. *J. Chem. Soc., Faraday Trans.* **1997**, *93*, 181.
(43) Aegerter, M. A.; Jafelicci, M., Jr.; Souza, D. F.; Zanotto, E. D. *Sol-Gel Science and Technology*; World Scientific Publishing Co. Pte Ltd.: Singapore, 1989.
(44) Nakamoto, K. *Infrared and Raman Spectra of Inorganic and Coordination Compounds*, 5th ed.; John Wiley & Sons, Inc.: New York, 1997.
(45) Deacon, G. B.; Phillips, R. J. *Coord. Chem. Rev.* **1980**, *33*, 227.
(46) Schubert, U. *J. Mater. Chem.* **2005**, *15*, 3701.
(47) Coluccia, S.; Tench, A. J. *Proceedings of the 7th International Congress on Catalysis*; Tokyo, Japan, 1980; p 1160.
(48) Hattori, H. *Chem. Rev.* **1995**, *95*, 537.

JP910538R